

Synthesis of Aza-*m*-Xylylene Diradicals with Large Singlet–Triplet Energy Gap and Statistical Analyses of Their EPR Spectra

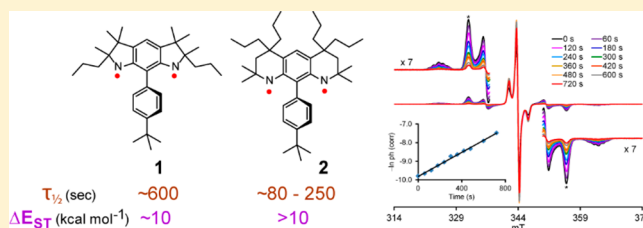
Arnon Olankitwanit,[†] Maren Pink,[‡] Suchada Rajca,[†] and Andrzej Rajca^{*,†}

[†]Department of Chemistry, University of Nebraska, Lincoln, Nebraska 68588-0304, United States

[‡]IUMSC, Department of Chemistry, Indiana University, Bloomington, Indiana 47405-7102, United States

S Supporting Information

ABSTRACT: We describe synthesis and characterization of a derivative of aza-*m*-xylylene, diradical **2**, that is persistent in solution at room temperature with the half-life measured in minutes (~80–250 s) and in which the triplet ground state is below the lowest singlet state by >10 kcal mol⁻¹. The triplet ground states and ΔE_{ST} of **2** in glassy solvent matrix are determined by a new approach based on statistical analyses of their EPR spectra. Characterization and analysis of the analogous diradical **1** are carried out for comparison. Statistical analyses of their EPR spectra reliably provide improved lower bounds for ΔE_{ST} (from >0.4 to >0.6 kcal mol⁻¹) and are compatible with a wide range of relative contents of diradical vs monoradical, including samples in which the diradical and monoradical are minor and major components, respectively. This demonstrates a new powerful method for the determination of the triplet ground states and ΔE_{ST} applicable to moderately pure diradicals in matrices.



1. INTRODUCTION

Recently, we reported triplet ($S = 1$) ground state aminyl diradical **1**, a derivative of aza-*m*-xylylene (Figure 1), that is persistent at room temperature and possesses a strong preference for the triplet ground state, in which the triplet state is below the lowest singlet state by a large singlet–triplet energy gap (ΔE_{ST}) ≈ 10 kcal mol⁻¹. Diradical **1** is remarkable, especially when compared to the well-known reactive intermediate *m*-xylylene diradical ($\Delta E_{ST} \approx 10$ kcal mol⁻¹),² which is observable in solution at room temperature for hundreds of nanoseconds.³ High-spin diradicals with large ΔE_{ST} that are far exceeding the thermal energy at room temperature ($\Delta E_{ST} \gg 0.6$ kcal mol⁻¹) are among the most effective building blocks for very high-spin polyradicals and magnetically ordered organic polymers.^{4–8} However, the breakthrough in purely organic magnets for practical technology applications relies on the development of high-spin radicals with $\Delta E_{ST} \gg 0.6$ kcal mol⁻¹ that are persistent at room temperature.^{9–12} Stable $S = 1$ diradicals (and $S > 1$ polyradicals) that are strongly paramagnetic at room temperature could also benefit the development of materials and agents such as organic paramagnetic contrast agents for magnetic resonance imaging (MRI),^{13,14} relaxation enhancement NMR spectroscopy,¹⁵ as well as spintronics and other applications.¹⁶

Diradical **1** is a planar derivative of aza-*m*-xylylene diradical in which the π -delocalization is largely limited to *m*-phenylene that maximizes the spin–spin interactions. In the search for stable diradicals with larger ΔE_{ST} , we consider the octahydroxypridoquinoline (OHPQ) diradical, for which Schreiner and co-workers predicted large $\Delta E_{ST} \approx 13.5$ kcal mol⁻¹.^{17,18}

We note that the OHPQ structure, with two six-membered rings annelated to *m*-phenylene, is analogous to diradical **1**, with five-membered rings annelated to *m*-phenylene. What would be the key factors affecting the larger ΔE_{ST} in OHPQ and whether the computational model is correct?

To gain insight, we set out to synthesize derivatives of OHPQ. Because a very large ΔE_{ST} is associated with large spin densities in the *m*-phenylene unit, the challenge lies in the design and synthesis of structures with adequate steric protection of those carbons with very large spin densities, while maintaining strong exchange coupling between the electron spins mediated by $2p_{\pi} - 2p_{\pi}$ interactions. Taking into account these demanding factors, we have developed an effective synthetic pathway to a sterically shielded OHPQ backbone, aminyl diradical **2** (Figure 2).

Here we report the synthesis and characterization of **2** and detailed characterization of **1**. We developed a new statistics-based approach for the determination of the triplet ground states and ΔE_{ST} for diradicals in glassy solvent matrices. In this approach, χT , the product of paramagnetic susceptibility and temperature, is measured multiple times by two methods: (1) double integration of the experimental and simulated EPR spectra providing χT as a function of ΔE_{ST} for the diradical/monoradical mixture and (2) the absolute measurement of χT by EPR spectroscopy using spin counting reference or by SQUID magnetometry. The difference between the resultant mean χT obtained by two methods is then tested for statistical significance to determine the triplet ground state and the

Received: August 7, 2014

Published: September 12, 2014

Half-life (295 K)	ΔE_{ST} , kcal mol ⁻¹ experimental computed
~100 ns	9.6 (NIPES, gas phase) 10.7-12.0 (BS-DFT) 11.3 (EOM-SF-CCSD) 11.0 (CASPT2N)
unknown	15.8-16.9 (BS-DFT)
unknown	13.5-14.2 (BS-DFT)
~10 min in 2-MeTHF	> 0.4 (2-MeTHF) 11.0-11.9 (BS-DFT), 1a (R = CH ₃) 9.6 (DDCI), 1a (R = CH ₃)

Figure 1. Triplet ground state diradicals: half-life at room temperature and singlet–triplet energy gap (ΔE_{ST}), determined experimentally by superconducting quantum interference device (SQUID) magnetometry or negative ion photoelectron spectroscopy (NIPES) and computationally by broken symmetry DFT (BS-DFT) and various correlated methods, e.g., DDCI.

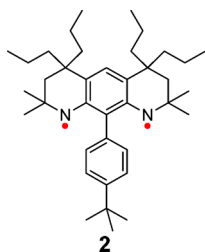


Figure 2. Aminyl diradical **2**.

lower bound ΔE_{ST} for **1** and **2** in 2-methyltetrahydrofuran (2-MeTHF).

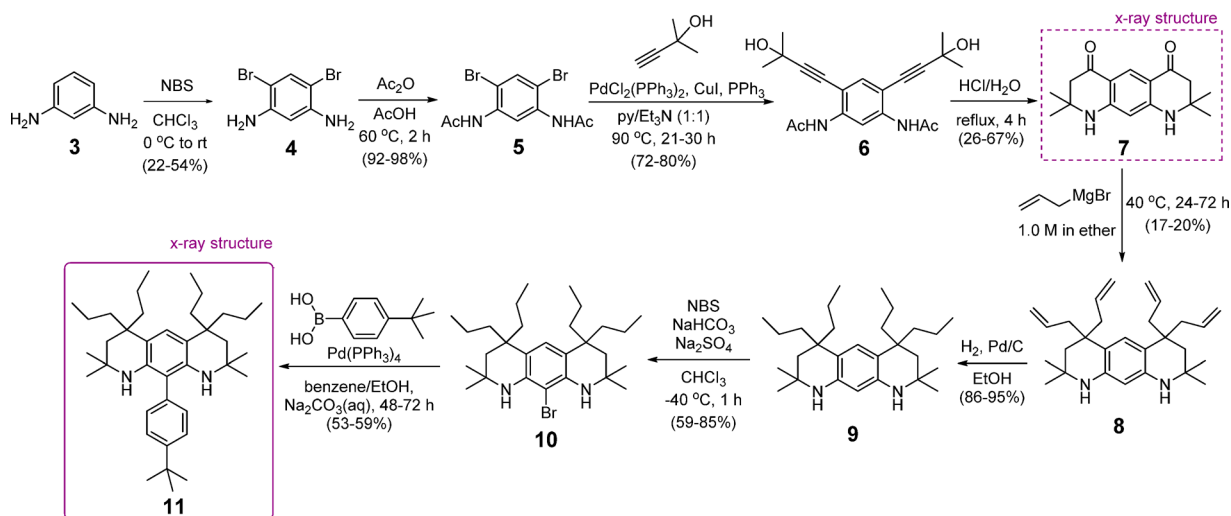
2. RESULTS AND DISCUSSION

Synthesis of Tricyclic Diamines: Precursors to Aminyl Diradical **2.** The synthesis of diamine **11** is outlined in Scheme 1. In the initial steps, 1,3-diaminobenzene is dibrominated and then *N*-acetylated to provide **5**, which is then subjected to Sonogashira cross-coupling. Product **6** of the Sonogashira cross-coupling is then refluxed with HCl/H₂O to result in the rearrangement of the propargylic alcohol to the enone, which is cyclized to give ultimately product **7**. Transformation of **6** to **7** was inspired by the Rupp-rearrangement/the Donnelly–Farrell cyclization to provide dimethyl-2,3-dihydro-1*H*-quinolin-4-one in a 90+% yield.^{19,20} Even considering that formation of **7** involves cyclization to two dimethyl-2,3-dihydro-1*H*-quinolin-4-one moieties, isolated yields for **7** are considerably lower and variable, in part due to poor solubility of **7** in common organic solvents. In the next step, **7** was treated with an excess of allyl Grignard reagent to produce *gem*-diallylation product **8**. Hydrogenation of **8** was followed by bromination,^{9,21} to give bromo-diamine **10**, which was then cross-coupled with 4-*tert*-butylphenyl boronic acid to provide the target diamine **11**.

X-ray Structures of **7 and **11**.** The structures of diketodiamine **7** and diamine **11** are confirmed by X-ray crystallography using synchrotron radiation (Figure 3 and Figures S1–S4, Supporting Information). As indicated by the torsion angles for both compounds (Table S3, Supporting Information), the lateral rings adopt half-chair conformations, though somewhat flattened, especially for **7**, compared to the half-chair of cyclohexene.²² The relative conformation of the half-chairs *syn*, i.e., diketodiamine **7** and the tricyclic fused ring moiety in diamine **11** have an approximate C_s point group. In **11**, the 4-*tert*-butylphenyl pendant, which is twisted out of the plane of the *m*-phenylene by the C11–C12–C29–C30 and C1–C12–C29–C34 torsion angles of 66.3(3)° and 64.2(3), breaks the approximate C_s-symmetry.

Determination of Diamine Structures Using NMR Spectroscopy and DFT-Computed NMR Chemical Shifts. The structure of the diamine **11**, precursor to diradical **2**, is confirmed by the assignment of its experimental ¹H and ¹³C

Scheme 1. Synthesis of Diamine **11**



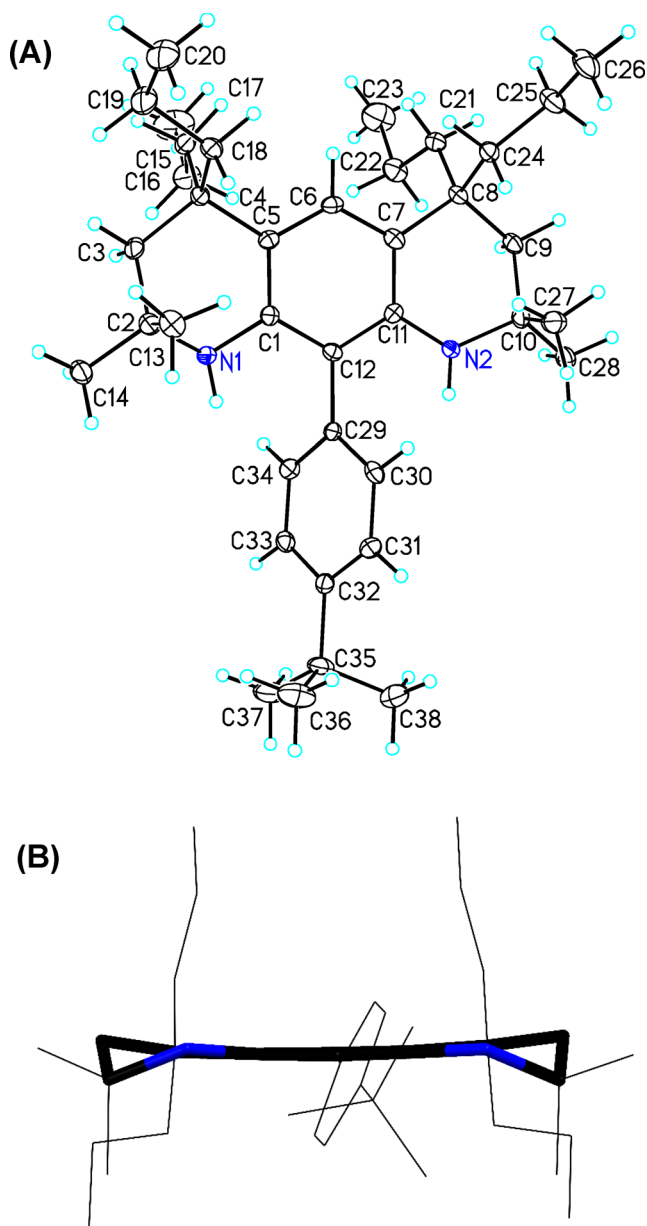


Figure 3. Molecular structure and conformation for diamine **11**. (A) top view of **11**; (B) side view of **11**. In the top view, carbon and nitrogen atoms are depicted with thermal ellipsoids set at the 50% probability level; disorder is omitted for clarity. In the side view, hydrogen atoms are omitted and the tricyclic fused ring moiety is shown in stick. Further details are reported in Tables S1–S3 and Figures S1–S4, Supporting Information.

NMR spectra in chloroform-*d* (or acetone-*d*₆) using standard 2D NMR spectroscopy, including ¹H–¹³C HSQC, ¹H–¹³C HMBC, ¹H–¹H NOESY, and ¹H–¹⁵N HSQC (Figures S5, S6, S10–S24, Supporting Information).²³ We also carried out the same characterization for diamine **12** (Figure 4), precursor to diradical **1**, but the assignments are incomplete because of the presence of two diastereomers (*meso*- and *dl*-isomers). Partial assignments are also carried out for **13** (Figure 4), the byproduct of the decomposition of diradical **2**.

Additional evidence for the structure is obtained from the correlation between the DFT-computed (δ_{DFT}) and experimental (δ_{expt}) ¹H and ¹³C NMR chemical shifts. The computations were carried out on the simplified structures of

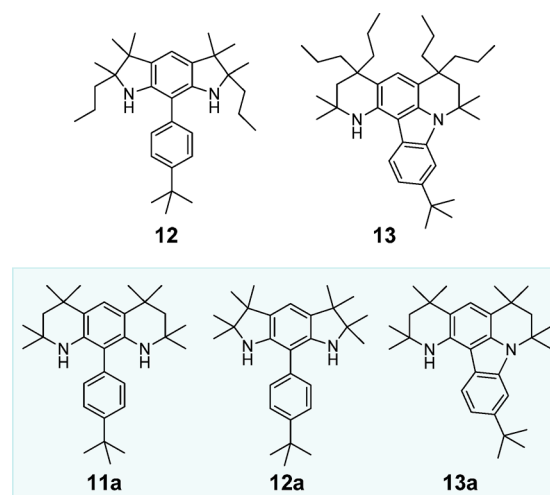


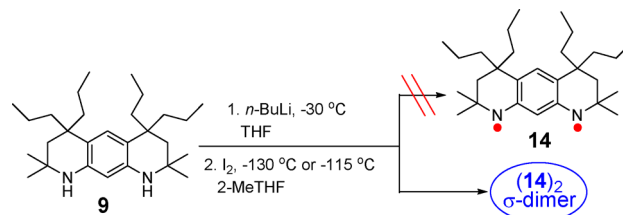
Figure 4. Diamines **12** and **13**, and simplified structures **11a**, **12a**, and **13a** for DFT-computations of NMR chemical shifts.

11–13, in which the *n*-propyl groups are replaced with methyl groups (**11a–13a**) (Figure 4). Geometries of simplified structures **11a–13a**, and tetramethylsilane were optimized at the B3LYP/6-31G(d,p) level of theory and confirmed as minima by vibrational analyses.^{24,25}

Linear regression of δ_{DFT} versus δ_{expt} provides coefficients of determination, $R^2 = 0.995–0.996$ and $0.991–0.999$, for ¹H and ¹³C NMR chemical shifts, respectively (Table S4, Supporting Information). The relationship between computed and experimental NMR chemical shifts is further illustrated by applying the correlations to scale linearly δ_{DFT} that provide δ_{scaled} , and then by plots of the differences between the scaled and experimental NMR chemical shifts ($\delta_{\text{scaled}} - \delta_{\text{expt}}$) for each distinct carbon or hydrogen atom in the structure (Figures S7–S9, Supporting Information). These plots confirm good agreement between theory and experiment, specifically the low-to-moderate values of statistical error parameters for ¹³C and ¹H NMR chemical shifts (Table S4, Supporting Information).^{23,26–29}

Generation of Aminyl Diradicals. We first attempted to prepare aminyl diradical **14** from diamine **9** (Scheme 2).

Scheme 2. Attempted Synthesis of Aminyl Diradical **14**: σ -Dimer (**14**)₂



Following the reaction conditions for generation of diradical **1**,¹ slight excess of *n*-BuLi over the stoichiometric amount of **2** equiv is added to **9**, the solvent is exchanged to 2-methyltetrahydrofuran (2-MeTHF), and then the reaction mixture is oxidized by iodine which is added by vacuum transfer in small portions.^{9,11,21} Because we expected that diradical **14** will be very reactive, we carried out the initial oxidation step at a lower temperature of -130 °C, instead of the typical temperature of -115 °C, to provide the spectrum in Figure 5.

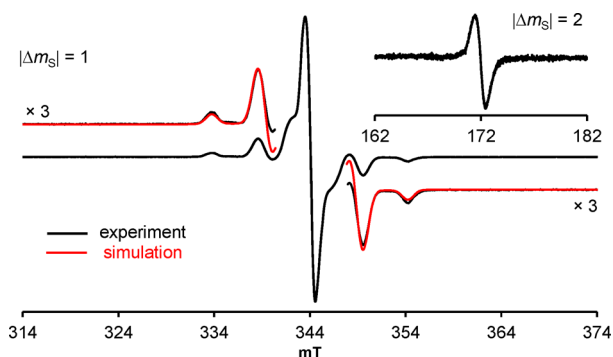


Figure 5. EPR (X-Band, $\nu = 9.6457$ GHz) spectrum at 132 K of the reaction mixture (2-MeTHF as solvent), resulting from addition of *n*-BuLi to diamine **9**, followed by addition of iodine, and allowing the reaction to proceed at 143 K (-130 °C) for 2 h. The simulation parameters for the $S = 1$ state ($|\Delta m_S| = 1$ region): $|D/hc| = 9.60 \times 10^{-3} \text{ cm}^{-1}$ ($|D/g\mu_B| = 10.3 \text{ mT}$), $|E/hc| = 0.30 \times 10^{-3} \text{ cm}^{-1}$ ($|E/g\mu_B| = 0.32 \text{ mT}$), $g_x = 2.0025$, $g_y = 2.0030$, $g_z = 2.0035$, Gaussian line ($L_x = 1.05$, $L_y = 1.15$, $L_z = 1.20 \text{ mT}$). Inset plot: $|\Delta m_S| = 2$ region.

The EPR spectrum of the reaction mixture shows an intense center peak, side bands, and a half-field ($|\Delta m_S| = 2$) transition (Figure 5). The side and half-field bands are the signature for a triplet state with a significant value for the zero-field splitting parameter D , thus suggesting the formation of a diradical. The g -tensor components average to the isotropic $g = 2.0030$, as expected for a nitrogen-centered radical with some spin density on carbon atoms. However, the spectral width for the triplet state, $2|D/g\mu_B| = 20.6 \text{ mT}$, as measured by the separation between the two outermost side bands, is much smaller than $2|D/g\mu_B| \approx 37 \text{ mT}$ in diradical **1** (Table 1). Because $2|D/g\mu_B|$ may be related to an “effective” distance (r in Å) between the radicals, $2|D/g\mu_B| \sim 2781g/r^3$, the spectral width of 20.6 mT is too small to originate from diradical **14**. In other words, the spectrum in Figure 5 would suggest relatively long $r \approx 6.5$ Å, compared to $r \approx 5.3$ Å for **1**.

For the reaction mixture shown in Figure 5, annealing at -115 °C for 1 h affects only slightly relative intensities of side and center bands in the EPR spectrum (Figure S37, Supporting Information). Examination of the annealed sample by superconducting quantum interference device (SQUID) magnetometry reveals a rather small paramagnetism, $\chi T \approx 0.18 \text{ emu K mol}^{-1}$, compared to $\chi T = 1.00 \text{ emu K mol}^{-1}$ expected for an $S = 1$ diradical **14** or to $\chi T = 0.75 \text{ emu K mol}^{-1}$ assuming that the exchange coupling between the radicals is negligible. These results indicate the presence of less than half of an unpaired electron per starting diamine **9**.

To rationalize the EPR spectrum and SQUID magnetic data, we consider that diradical **14** may form either a σ - or a π -dimer. A π -dimer like structure for aminyl diradical such as **14** is expected to provide much greater EPR spectral width—several

times greater than that experimentally observed in Figure 5, and a much greater value of χT by SQUID magnetometry than the experimentally determined $\chi T \approx 0.18 \text{ emu K mol}^{-1}$. For example, π -dimer-like structures formed from aminyl diradical **15** and tetraradicals **16** and **17** (Figure 6) had significantly increased EPR spectral widths, compared to those for corresponding monomer structures. These large spectral widths were accounted for by D tensor addition.^{9,11} Specifically, for a planar, $S = 1$ ground state aminyl diradical, which has the largest component of D tensor along the axis of the $2p_\pi$ orbitals at the nitrogen atoms as in **1** and **2** (see: next section), the EPR spectrum of a π -dimer-like structure is expected to show a thermally populated $S = 2$ state with a spectral width exceeding that of the $S = 1$ monomer.⁹

The σ -dimer is expected to involve the formation of σ -bonds between the atoms with large, sterically unshielded spin densities in diradical **14**.^{30–33} Using a simplified structure such as diradical **14a**, derived from **14** by replacing the *n*-propyl groups with methyl groups, triplet states of σ -dimers with CN and NN bonds were modeled at the UB3LYP/6-31G(d)+ZPVE level (Table S16, Supporting Information). The $N\cdots N$ and $C\cdots N$ distances between atoms with large Mulliken atomic spin densities (0.5–0.6 au) range from 3.4 to 6.8 Å. In diradicals **14a** and **2a** (Table 5), the computed $N\cdots N$ distances are 4.68 and 4.74 Å, and a significant fraction of spin density is located, in close proximity, within the *m*-phenylene unit.

In summary, the attempted generation of diradical **14** resulted in reaction mixtures containing only a small fraction of the expected radicals, which provide EPR spectra with much narrower than expected spectral width. These results suggest that diradical **14** may not be persistent even at -130 °C by decaying through the formation of covalently bonded dimers (and perhaps oligomers).

Diradicals 1 and 2. Aminyl diradicals **1** and **2** are prepared from the corresponding diamines, as previously reported for **1**.¹ (A similar protocol was also developed for aminyl tetraradicals.¹¹)

As illustrated for diradical **2** (Scheme 3), the diamine **11** ($\sim 1 \mu\text{mol}$) is treated with *n*-BuLi to provide an orange solution of the corresponding dianion in THF/hexane. After solvent exchange to 2-MeTHF, iodine is added in small portions by vacuum transfer to the solution of the dianion at -115 °C (158 K); after each addition of iodine, the green reaction mixture is monitored by EPR spectroscopy at 132–133 K to observe the formation of diradical **2**.

This protocol provides samples of diradical **1**, for which the diamine is almost completely converted to the diradical/monoradical mixture with a molar fraction of **1** of $\sim 85\%$. In contrast, samples of diradical **2** are typically 40:60–50:50 mixtures of diradical and monoradical.

Increasing both the temperature and reaction time of diamine with *n*-BuLi did not improve the yield of **2**. The

Table 1. Summary of Experimental EPR Spectra for the Aminyl Diradicals in 2-MeTHF at 132–133 K and Computed EPR Spectra at the B3LYP/EPR-II Level^a

diradical	experiment									calculation		
	conc. ^b (mM)	ν (GHz)	$ D/hc $	$ E/hc $	$ A_{zz}/2hc $	g_x	g_y	g_z	g	D/hc	E/hc	$A_{zz}/2hc$
1	9	9.4780	17.49	3.60	1.13	2.0046	2.0030	2.0019	2.0032	34.4	0.02	1.13
2	5	9.6415	17.94	1.42	1.08	2.0050	2.0031	2.0018	2.0033	35.9	0.80	1.16

^aBoth experimental and calculated values of $|D/hc|$, $|E/hc|$, and $|A_{zz}/2hc|$ are reported in 10^{-3} cm^{-1} . ^bConcentrations are based on the mass of precursor diamine for diradicals **1**, **2** and volume of the solvent; parameters for **2** are after the sample, shown in Figure 7, was diluted with 2-MeTHF.

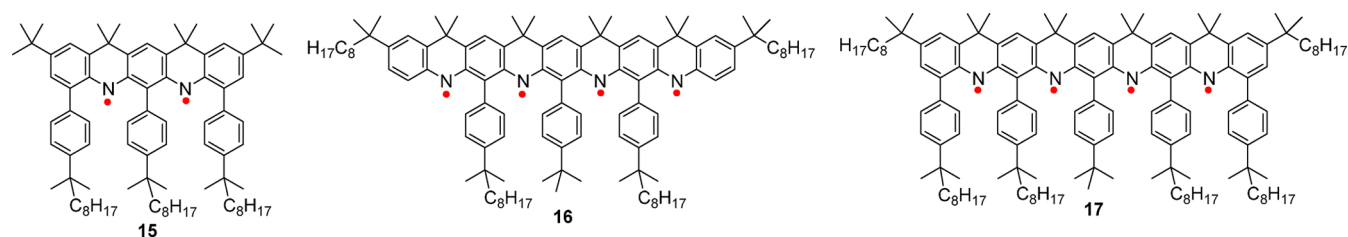
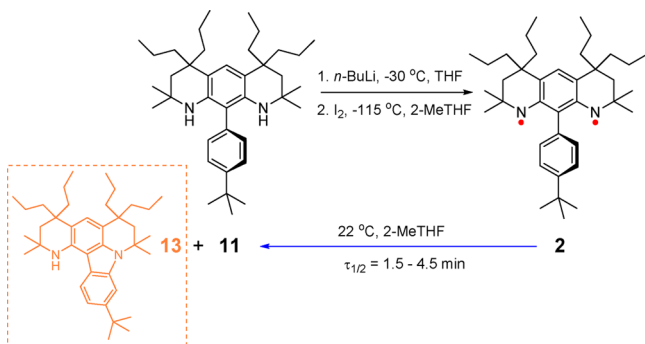


Figure 6. Structures of aminyl diradical and tetradiradicals forming π -dimer-like structures.

Scheme 3. Synthesis of Aminyl Diradical 2 and Its Decay at Room Temperature in 2-Methyltetrahydrofuran to Diamine 11 and Byproduct 13^a



^aThe ratio of 13 to 11 ranged from 0.63 to 2.87.

oxidation using iodine, followed by the stronger oxidant such as $[\text{Cp}_2\text{Fe}]^+[\text{BF}_4]^-$, provided one sample of **2** as a 60:40 mixture of diradical and monoradical (Figure S29, Supporting Information), but we found this result difficult to reproduce. Direct oxidation of the dianion with various oxidants did not produce detectable **2** (Table S19, Supporting Information).

Successful preparation of diradical **2** and the failure to detect diradical **14**, using similar reaction conditions, suggests that the carbon and nitrogen atoms with significant spin densities have to be sterically shielded by a large group such as the 4-*tert*-butyl-phenyl pendant.

EPR Spectroscopy. EPR spectra of **1**¹ and **2** in 2-MeTHF at 132 K consist of six side bands in the $|\Delta m_s| = 1$ region and a half-field ($|\Delta m_s| = 2$) transition, indicating a triplet state with significant *D* and *E* zero-field splitting parameters (Figure 7). The two outermost bands (*Z*-turning points) are split into broadened pentuplets with $|A_{ZZ}/2hcl|$ spacings, where A_{ZZ} is the largest principal value of the ¹⁴N hyperfine tensor (the *A* tensor) of two nitrogen nuclei.³⁴ Because the largest principal value of the ¹⁴N hyperfine tensor is expected to coincide with the direction of the nitrogen 2p_π orbital,³⁵ the 2p_π orbital in the diradical can be considered to be approximately parallel to the *Z*-axis, which is the direction of the largest principal value of the *D* tensor. Assuming that the *D* tensor primarily originates in the magnetic dipole–dipole interactions,³⁶ these relative orientations of *D* and *A* tensors in the aminyl diradicals **1** and **2** suggest an “oblate-like” shape of spin density that is compressed in the direction of the *Z*-axis.¹

The tensor orientations and an “oblate-like” shape of spin density in **1** and **2** are similar to those in diazapentacene-based aminyl diradicals, and are in contrast to analogous nitroxides with a “prolate-like” shape of spin density.^{1,9,37}

Decay Kinetics of Aminyl Diradicals. The persistence of **1** and **2** in 2-MeTHF was investigated by EPR spectroscopy. A typical procedure is illustrated using a sample of ~5 mM

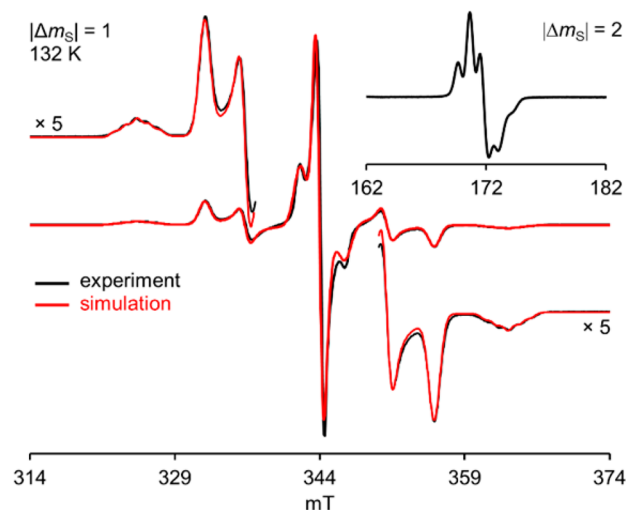


Figure 7. EPR (X-Band, $\nu = 9.6463$ GHz) spectra of 19 mM aminyl diradical **2** in 2-MeTHF at 132 K. The simulation parameters for the $S = 1$ state are $|D/hcl| = 17.94 \times 10^{-3} \text{ cm}^{-1}$, $|E/hcl| = 1.42 \times 10^{-3} \text{ cm}^{-1}$, $|A_{ZZ}/2hcl| = 1.08 \times 10^{-3} \text{ cm}^{-1}$, $g_x = 2.0050$, $g_y = 2.0031$, $g_z = 2.0018$, Gaussian line ($L_x = 0.95$, $L_y = 1.17$, $L_z = 0.97$ mT). The center lines correspond to an $S = 1/2$ (monoradical) byproduct simulated with identical *g*-components and $|A_{ZZ}/hcl| = 2.25 \times 10^{-3} \text{ cm}^{-1}$, using Gaussian line ($L_x = 0.75$, $L_y = 0.70$, $L_z = 1.35$ mT). (This sample was later diluted with 2-MeTHF at low temperature for magnetic susceptibility measurements, Table 3 (Sample 1), Figure S25, Supporting Information.)

diradical **2** (Figure 8, and sample 2 in Table 2). First, the diradical is annealed at 246 K to remove any excess of I_2 ; for this sample of **2**, the EPR spectra before and after annealing for 1 h were identical (Figure S30, Supporting Information). However, the decay of the diradical was readily detectable at 295 K, where the EPR spectra indicate first order kinetics with a half-life, $\tau_{1/2} \approx 214$ s (Figure 8); two other samples of **2** showed half-lives of 246 and 80 s, where the sample with the shorter half-life possessed a considerable amount of iodine based upon prior annealing at 246 K (Table 2, Figure S34, Supporting Information). These half-life values are considerably shorter than $\tau_{1/2} \approx 600$ s for diradical **1** under similar conditions (Table 2).

After several days of annealing samples of **1** at room temperature, ¹H NMR spectra and mass spectrometry showed that the isolated samples were predominantly starting diamine **12**.¹ These results suggest that the decay of **1** to **12** in 2-MeTHF proceeds by a hydrogen abstraction mechanism,³⁸ which is analogous to those observed for matrix isolated acene-based aminyl diradical **15** and aminyl tetradiradical **17**.^{9,11} In contrast for **2**, its crude reaction mixtures, obtained after several days of annealing samples of **2** at room temperature, contained not only starting diamine **11** but also a significant amount of a

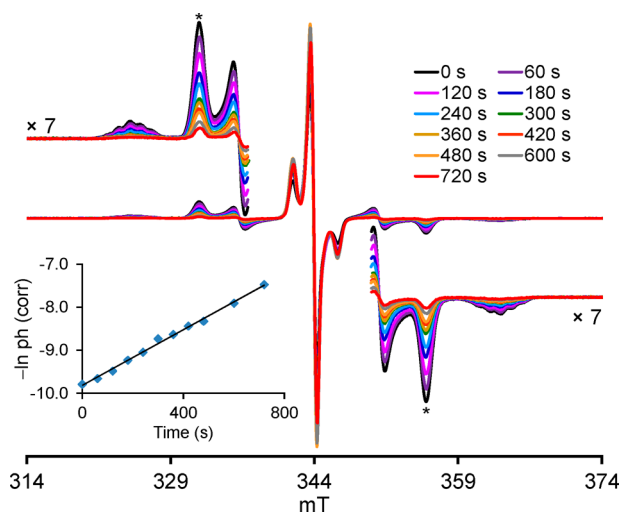


Figure 8. Decay kinetics for 5.1 mM diradical **2** in 2-MeTHF at room temperature: for the peaks at ~ 332 and 356 mT, asterisks indicate the peaks plotted in the inset plot as $-\ln \text{ph (corr)}$ vs time, where “ph (corr)” corresponds to averaged peak heights for which intensities were corrected with the nitroxide reference (1.0 M TEMPONE).

byproduct **13** (Scheme 3, Table S12, Figures S35, S39, S42, Supporting Information); the highest ratio of **13** to **11**, among the three samples used for kinetics of **2**, corresponded to a sample of **2** with the lowest value of $\tau_{1/2} \approx 80$ s (Table S12, Supporting Information). These results suggest that the additional pathway for the decay of diradical through byproduct **13** is responsible for relatively low values of $\tau_{1/2}$ for **2**, compared to those for **1**. Although we suspect that the residual iodine may contribute to the observed distribution of the decay rates, understanding of the decay rates for diradical **2** requires further studies.

We computed energy minima along a plausible pathway leading from diradical **2** to byproduct **13**, using simplified structures **2a** and **13a**, in which *n*-propyl chains are replaced with methyl groups (Scheme 4, Table S15, Supporting Information).

The reaction starting from triplet diradical **2a** to diamagnetic byproduct **13a** is remarkably exothermic (-56.1 kcal mol $^{-1}$).

For **2**, we investigated its reaction with oxygen (O_2). The EPR spectrum of ~ 13 mM **2** in 2-MeTHF lost much of its intensity, in particular, the complete disappearance of the triplet resonances for **2** was observed, after the solution is saturated with dry O_2 at 165 K (-108 °C) for 15 min (and then degassed) (Figures S43–S46, Supporting Information). This behavior is analogous to that observed upon exposure of **1** in 2-MeTHF to O_2 .¹

Determination of the Ground State and ΔE_{ST} for Diradicals **1 and **2**: Statistical Analyses of Mean χT .** After

the optimization of reaction conditions, the generation of the diradicals **1** and **2** from the corresponding diamines **12** and **11** produces the crude reaction mixtures in 2-MeTHF that contain a significant content of monoradicals. For **1**, however, selected samples with high content of diradical ($\sim 85\%$) could be prepared in SQUID/EPR sample tubes, thus enabling determination of the triplet state and the lower limit of ΔE_{ST} using SQUID magnetometry via the detection of thermal population of the m_s -levels and electronic states with different values of S .¹ For **2**, the best samples had only moderate content of diradical (~ 40 – 50%), thus precluding reliable determination of the ground state and lower limit of ΔE_{ST} by SQUID magnetometry.

To determine the triplet ground state and ΔE_{ST} , we measure χT , the product of paramagnetic susceptibility (χ) and temperature (T), multiple times for the same sample of diradical by two methods. In the first method, we obtain an estimated χT as a function of ΔE_{ST} , i.e., χT_{Int} using double integrated intensities for diradical and monoradical in the experimental EPR spectra for the diradical/monoradical mixture (eqs 1 and 2). Simulated EPR spectra are used to resolve spectral overlaps between diradical and monoradical.

$$\chi T_{\text{Int}} = (\text{Int}_{\text{D}} + \text{Int}_{\text{M}}) / [(\text{Int}_{\text{D}}/\chi T_{\text{D}}) + (\text{Int}_{\text{M}}/0.375)] \quad (1)$$

$$\chi T_{\text{D}} = 3 / [3 + \exp((-2J/k)/T)] \quad (2)$$

In eq 1, Int_{D} and Int_{M} are double integrated EPR intensities for diradical and monoradical, respectively; in the denominator of eq 1, these intensities are scaled by corresponding χT in the units of emu K mol $^{-1}$ such as monoradical (0.375) and diradical (χT_{D}) with a singlet–triplet energy gap of $2J/k$ (eq 2).

In the second method, we measure total χT for the sample (χT_{EPR}) by EPR spectroscopy using a spin counting standard (eq 3) or by SQUID magnetometry.

$$\chi T_{\text{EPR}} = \{[\text{std}]/[\text{sample}]\} \times \{\text{Int}_{\text{sample}}/\text{Int}_{\text{std}}\} \times \{(1/2) \times S(S+1)_{\text{std}}\} \quad (3)$$

To ensure that the multiple EPR measurements of χT are independent, the sample is thawed in a low temperature bath (-115 °C), following each measurement of χT , and then before the next measurement of χT , the sample is carefully frozen in a liquid nitrogen bath prior to the insertion of the sample to the EPR cavity.

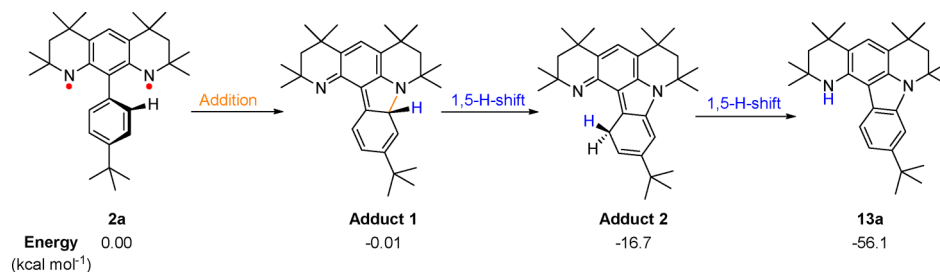
These measurements provide two sets of χT data for each sample. For a given sample, the difference between the resultant mean χT of each of the two sets is then tested for statistical significance, to determine the triplet ground state and ΔE_{ST} for **1** and **2** in 2-methyltetrahydrofuran.

Table 2. Decay Kinetics for Diradicals **1** and **2** in 2-MeTHF at Room Temperature

diradical	sample	n^a	R^2	k (s $^{-1}$) ^c	SEM (k)	P (k)	t (k)	95% confidence limits (k)			
								lower (s $^{-1}$)	upper (s $^{-1}$)	SEM ($\tau_{1/2}$) ^b	$\tau_{1/2}$ ^c
1	1	6	0.9750	$(1.11 \pm 0.25) \times 10^{-3}$	8.899×10^{-5}	2.364×10^{-4}	12.49	0.0008644	0.001359	49.93	624 ± 138.6
2	1	9	0.9792	$(2.81 \pm 0.37) \times 10^{-3}$	1.551×10^{-4}	3.833×10^{-7}	18.14	0.002447	0.003180	13.58	246 ± 32.1
2	2	10	0.9946	$(3.26 \pm 0.16) \times 10^{-3}$	8.522×10^{-5}	2.401×10^{-10}	38.24	0.003063	0.003456	5.56	214 ± 12.8
2	3	6	0.9567	$(8.67 \pm 2.56) \times 10^{-3}$	9.221×10^{-4}	7.146×10^{-4}	9.40	0.006105	0.01123	8.51	80 ± 23.6

^aNumber of data points. ^bSEM($\tau_{1/2}$) = $\tau_{1/2}[\text{SEM}(k)/k]$. ^cMean \pm 95% confidence interval.

Scheme 4. B3LYP/6-31G(d)//B3LYP/6-31G(d) Relative Energies after ZPVE Correction



Using a two-tailed two-sample *t* test for means with unequal variances (Welch variant of *t* test), we compare the mean χT_{Int} with either the mean χT_{EPR} (for **2**) or the mean χT_{SQUID} (for **1**), to identify the differences between the means that would be significant at a probability $P < 0.05$ and $P < 0.01$. (In the nomenclature of statistics, “two-sample” implies two means such as χT_{Int} and χT_{EPR} that are being compared; these two means are obtained for the same sample of the diradical.)

As illustrated for **2**, the difference between mean χT_{EPR} and χT_{Int} ($2J/k = 0$ K) is very significant with a probability $P = 10^{-6}$ – 10^{-3} , indicating unequivocally a triplet ground state (Table 3). The difference is significant at a probability $P < 0.05$ when $2J/k = 800$, 260, or 230 K; at a lower, more significant, probability, $P < 0.01$, smaller values of $2J/k = 350$, 220, and 110 K are obtained. We interpret these results as the lower bounds for the singlet–triplet gaps, $2J/k$, i.e., $2J/k > 800$ K and > 350 K with a 95 and 99% confidence level, respectively.

Analogous analyses for diradical **1**, based upon SQUID data (Table 4), confirm the triplet ground state with an exceedingly strong statistical significance ($P = 10^{-44}$ – 10^{-10}) and provide the lower bounds for the singlet–triplet gaps, $2J/k > 395$ K and > 386 K, at a 95 and 99% confidence level, respectively.

In summary, we developed a new powerful method for the determination of the triplet ground states and ΔE_{ST} applicable to moderately pure diradicals in matrices. Using this method, triplet ground states for **1** and **2** are determined with strong statistical significance with probabilities of $P \approx 10^{-44}$ – 10^{-3} . Also, a considerably elevated lower bound for $\Delta E_{\text{ST}} = 0.8$ kcal mol⁻¹ in **1** is found, compared to 0.4 kcal mol⁻¹ obtained previously by direct SQUID measurements. In **2**, a much more elevated lower bound for $\Delta E_{\text{ST}} = 1.6$ kcal mol⁻¹ is determined.

DFT Computation of Singlet–Triplet Energy Gaps and EPR Tensors. The simplified structures of aminyl diradicals **1**, **2**, and **14**, i.e., **1a**, **2a**, and **14a** (Table 5), were studied at the UB3LYP/6-31G(d)+ZPVE, UB3LYP/6-311+G(d,p)+ZPVE, and UM06-2X/6-31G(d)+ZPVE levels of theory. Geometries were optimized for both triplet and broken-symmetry (BS) singlet states. Conformations of the lateral rings of the fused tricyclic moieties are oriented “anti”, i.e., **14a** has anti-half chairs and the C_2 point group of symmetry. In **1a** and **2a**, the fused tricyclic moieties have an approximate C_2 point group of symmetry.

The singlet–triplet energy gap (ΔE_{ST}) may be estimated using the energy difference between ground state triplet and BS singlet (ΔE_{UHF}) and the correction for spin contamination (eq 4).^{39–41} The correction for spin contamination is based on the calculated mean values of the S^2 operator for the ground state triplet ($\langle S^2_{\text{T}} \rangle$) and BS singlet ($\langle S^2_{\text{BS-S}} \rangle$).

$$\Delta E_{\text{ST}} = \Delta E_{\text{UHF}}[\langle S^2_{\text{T}} \rangle / (\langle S^2_{\text{T}} \rangle - \langle S^2_{\text{BS-S}} \rangle)] \quad (4)$$

Diradical **2a** and diradical **14a** possess similar $\Delta E_{\text{ST}} \approx 14$ kcal mol⁻¹, as expected because the spin density in **2a** is predominantly confined to the aza-*m*-phenylene moiety (Figure 9), and for **1a**, lower ΔE_{ST} by 2–3 kcal mol⁻¹ is found at the same level of theory. Although in *m*-xylylene, the newer M06-2X functional was found to be superior among DS-DFT methods for the computation of ΔE_{ST} ,⁴² both B3LYP and M06-2X functionals perform similarly for our derivatives of aza-*m*-xylylene. Most likely, our BS-DFT-computed values of ΔE_{ST} are somewhat overestimated.^{41,42} As mentioned in the introduction (Figure 1), Barone and co-workers’ computation of **1a** at a much higher level of theory (DDCI) provided $\Delta E_{\text{ST}} \approx 9.6$ kcal mol⁻¹,^{18d} which is about 2 kcal mol⁻¹ below the BS-DFT results in Table 5.

Using the UB3LYP/6-311+G(d,p)-optimized geometries of the triplet ground state of **2a**, computations of EPR *D*-tensor and ¹⁴N *A*-tensors at the B3LYP/EPR-II level using ORCA^{43,44} were carried out analogously to the previously reported computations of **1a**.¹ The B3LYP/EPR-II-computed EPR spectra of **2a** provide the correct orientation of the *D*-tensor (and thus, the correct sign), as indicated by the ¹⁴N pentuplet splitting of the outermost lines (Z-lines), similarly to **1a** and other planar aminyl diradicals. However, as in **1a** and other planar aminyl diradicals, the value of the zero-field splitting parameter $D \approx 36 \times 10^{-3}$ cm⁻¹ in **2a** is overestimated by a factor of about two (Table 1).

3. CONCLUSION

We successfully synthesized the diradical derivative of OHPQ, which was predicted to possess a large $\Delta E_{\text{ST}} \approx 13.5$ kcal mol⁻¹. The aminyl diradical **2**, with sterically shielded OHPQ backbone, is persistent in solution at room temperature with a half-life measured in minutes (~80–250 s). An approach based on statistical analyses of EPR spectra of moderately pure diradicals in matrices provides a new powerful method for the determination of the triplet ground states and ΔE_{ST} . In contrast, the current gold standard determinations of triplet ground state and ΔE_{ST} for diradicals in glassy solvent matrices, such as SQUID magnetometry, require nearly pure samples of diradicals, a difficult task, because reactive diradicals are commonly analyzed as crude reaction mixtures. We found that **2** in a glassy solvent matrix possesses triplet ground state with $\Delta E_{\text{ST}} > 1.6$ kcal mol⁻¹, in qualitative agreement with the BS-DFT theory predicting $\Delta E_{\text{ST}} \approx 14$ kcal mol⁻¹. Indeed, the diradical derivative of OHPQ, with six-membered rings annelated to aza-*m*-xylylene surpasses ΔE_{ST} in the analogous diradical with five-membered rings, presumably due to slightly greater delocalization of spin density into the *m*-phenylene.

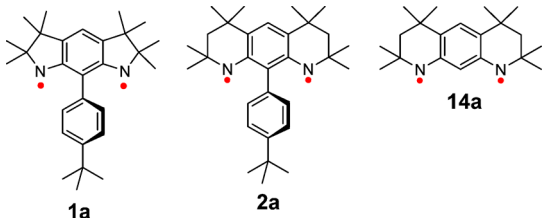
Table 3. Statistical Analyses of χT for Diradical 2

	sample 1				sample 2				sample 3			
	$\chi T_{\text{inv}} 2J/k$ (K)				$\chi T_{\text{inv}} 2J/k$ (K)				$\chi T_{\text{inv}} 2J/k$ (K)			
	χT_{EPR}	0	800	350	χT_{EPR}	0	260	220	χT_{EPR}	0	230	110
	0.689065906	0.594778856	0.696607073	0.68854741	0.633768071	0.562160853	0.629778997	0.625462092	0.63393631	0.573130625	0.643214825	0.619387924
	0.703050268	0.593843967	0.695005984	0.687004416	0.639418142	0.56133831	0.628525264	0.624238009	0.711951236	0.574857601	0.645841358	0.62169164
	0.727747543	0.594110236	0.695461758	0.68744367	0.62808763	0.561341156	0.6285296	0.624242243	0.700414189	0.574613003	0.645469012	0.62136516
	0.715999177	0.594249017	0.695699386	0.68767268	0.648477088	0.561168276	0.62826626	0.62398512	0.679068858	0.57465828	0.645537928	0.621425589
	0.707348613	0.594356428	0.695883334	0.687849953	0.644752536	0.560219575	0.626822194	0.622575083	0.690334582	0.573943549	0.644450492	0.620471928
	0.714391678	0.594373953	0.695913351	0.687878881	0.631063782	0.562230955	0.629885909	0.625566472				
n	6	6	6	6	6	6	6	6	5	5	5	5
mean	0.709600531	0.59428541	0.695761815	0.687732835	0.637594542	0.561409854	0.628634704	0.624344836	0.683141035	0.574240612	0.644902723	0.620868448
SD	0.013136664	0.000310887	0.000532429	0.00051311	0.008008324	0.000737993	0.001124179	0.001097635	0.030074176	0.000709597	0.001079203	0.000946567
SEM	0.005363021	0.000126919	0.000217363	0.000209476	0.003269385	0.000301284	0.000458944	0.000448108	0.01344958	0.000317342	0.000482634	0.000423318
P	3.99926×10^{-06}	0.0493823	0.009531851		2.34733×10^{-06}		0.040424392	0.009432841		0.001259964	0.046667913	0.009777294

Table 4. Statistical Analyses of χT for Diradical 1^a

	sample 1				sample 2				sample 3							
	$\chi T_{\text{inv}} 2J/k$ (K)				$\chi T_{\text{inv}} 2J/k$ (K)				$\chi T_{\text{inv}} 2J/k$ (K)							
	$\chi T_{\text{SQUID}} H = 3 \text{ T}$	0	395	386	$\chi T_{\text{SQUID}} H = 0.5 \text{ T}$	0	372	364	$\chi T_{\text{SQUID}} H = 3 \text{ T}$	0	303	279	$\chi T_{\text{SQUID}} H = 0.5 \text{ T}$	0	302	276
n	29	4	4	4	36	4	4	4	29	4	4	4	53	4	4	4
mean	0.89714	0.706892	0.894984	0.894097	0.894700	0.7068920	0.892596	0.891667	0.889214	0.706330	0.881423	0.876570	0.888920	0.706330	0.881237	0.875903
SD	0.00328	0.000703	0.001395	0.001391	0.003187	0.0007035	0.001385	0.001382	0.005439	0.002693	0.005139	0.005062	0.005561	0.002693	0.005136	0.005051
SEM	0.00061	0.000352	0.000697	0.000696	0.000531	0.0003517	0.000692	0.000690	0.01010	0.001347	0.002570	0.002531	0.000764	0.001347	0.002568	0.002526
P	5.16×10^{-44}	0.0459	0.00971		1.36×10^{-41}	0.0451	0.00941		1.12×10^{-12}	0.0479	0.00962		3.92×10^{-10}	0.0471	0.00970	

^aComplete version of this table, including the raw data, is provided in the Supporting Information (Table S8).

Table 5. DFT-Computed Singlet-Triplet Energy Gaps (ΔE_{ST})^a


diradical	BS-DFT+ZPVE level	ΔE_{UHF} (kcal mol ⁻¹)	ΔE_{ST} (kcal mol ⁻¹)
1a	UB3LYP/6-31G(d) ^b	6.12	11.58
	UB3LYP/6-311+G(d,p) ^b	5.86	11.03
	UM06-2X/6-31G(d)	6.25	11.94
2a	UB3LYP/6-31G(d)	7.19	14.15
	UB3LYP/6-311+G(d,p)	7.09	13.96
	UM06-2X/6-31G(d)	7.51	14.79
14a ^c	UB3LYP/6-31G(d)	7.34	14.40
	UB3LYP/6-311+G(d,p)	7.17	14.09
	UM06-2X/6-31G(d)	7.11	13.96

^aOptimized geometries and zero-point vibrational energy correction for the triplet and broken-symmetry singlet. ^bRef 1. ^cC₂-symmetric conformation (*anti*-half-chairs) of diradical 14a was computed. Further details may be found in Table S14, Supporting Information.

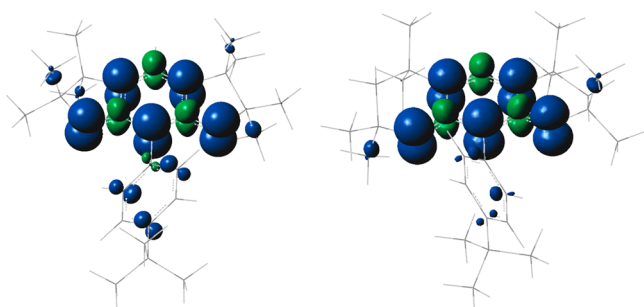


Figure 9. Spin density maps for the triplet ground states of diradicals 1a¹ and 2a at the UB3LYP/EPR-III//UB3LYP/6-311+G(d,p) level of theory. Positive (blue) and negative (green) spin densities are shown at the isodensity level of 0.006 electron/Bohr³.

4. EXPERIMENTAL SECTION

X-ray Crystallography. Crystals of 7 and 11 for X-ray studies were prepared by slow evaporation from solutions in organic solvents. Data collections were performed at the Advanced Photon Source, Argonne National Laboratory in Chicago, using synchrotron radiation ($\lambda = 0.41328 \text{ \AA}$). Final cell constants were calculated from the xyz centroids of strong reflections from the actual data collection after integration (SAINT);⁴⁵ intensity data were corrected for absorption (SADABS).⁴⁶ The space groups were determined based on intensity statistics and systematic absences. The structures were solved with direct methods using Sir2004⁴⁷ and refined with full-matrix least-squares/difference Fourier cycles using SHELXL-97.⁴⁸ All non-hydrogen atoms were refined with anisotropic displacement parameters. The hydrogen atoms were placed in ideal positions and refined as riding atoms with relative isotropic displacement parameters, with the following exceptions: (1) in diketone-diamine 7, the hydrogen atoms involved in hydrogen bonding (Table S2, Supporting Information) were refined for all parameters and (2) in diamine 11, the hydrogen atoms bound to nitrogen were refined independently. Crystal and structure refinement data for 7 and 11 are in the Supporting Information and the accompanying file in CIF format.

Synthesis. Standard techniques for synthesis under inert atmosphere (argon or nitrogen), using custom-made Schlenk glassware, custom-made double manifold high vacuum lines, and argon-filled Vacuum Atmospheres gloveboxes, were employed. Chromatographic separations were carried out using normal phase silica gel. For selected diamines, determination of R_f values was carried out using TLC plates which were deactivated using 3% Et₃N in pentane.⁴⁹ The preparation of compound 5 is described in the Supporting Information.

Preparation of 6. 1,3-Dibromo-4,6-bis(acetamido)benzene 5 (0.2027 g, 0.579 mmol, 1 equiv) was weighed, transferred to a Schlenk vessel equipped with a magnetic stir bar and evacuated under a high vacuum for 1 h. A solution of Et₃N/pyridine (1:1, 0.1 M, bubbled with nitrogen gas for 10 min) was added to the reaction Schlenk vessel under nitrogen gas. 2-Methyl-3-butyn-2-ol (0.17 mL, 1.74 mmol, 3 equiv) was added and the solution was stirred at room temperature for 10 min. PPh₃ (0.1519 g, 0.579 mmol, 1 equiv), CuI (11.0 mg, 0.0579 mmol, 0.1 equiv) and PdCl₂(PPh₃)₂ (40.6 mg, 0.0579 mmol, 0.1 equiv) were weighed and added to the reaction Schlenk vessel under nitrogen flow to produce a yellow suspension. The reaction was stirred for 30 h at 90 °C, under the exclusion of light. The resultant orange suspension was cooled down to room temperature, filtered through a Celite plug with ethyl acetate. The filtrate was evaporated under reduced pressure. A small amount of heptane was added and evaporated in vacuo to give a light yellow powder. The powder was washed with dichloromethane (2 × 5 mL) to provide diamine 6 (165.0 mg, 80%) as a light yellow powder. mp 210–212 °C (under air, decomposed to deep orange liquid). ¹H NMR (600 MHz, dimethyl sulfoxide-*d*₆): $\delta = 9.031$ (s, 2H), 8.398 (s, 1H), 7.327 (s, 1H), 5.523 (s, 2H), 2.106 (s, 6H), 1.484 (s, 12H). ¹³C NMR (150 MHz, dimethyl sulfoxide-*d*₆): $\delta = 168.37, 139.14, 134.13, 134.05, 116.13, 110.68, 101.78, 75.77, 63.85, 23.81$. IR (cm⁻¹): 3346, 3232, 2978, 1664, 1581, 1539, 1505, 1413, 1361, 1263, 1162, 956, 890, 689. HR-ESI MS (0.05% NaOAc in MeOH/H₂O (3:1)): m/z ion type (%RA for $m/z = 370\text{--}380$): 379.1616 [M + Na]⁺ (100%, -4.7 ppm for ¹²C₁₀¹H₂₄¹⁴N₂¹⁶O₄²³Na₁).

Preparation of 7. Our procedure follows previous reports on the preparation of 2,2-dimethyl-2,3-dihydro-1H-quinolin-4-one.¹⁹ Diamine 6 (0.231 g, 0.649 mmol, 1 equiv) was transferred to a 25 mL round-bottom flask equipped with a magnetic stir bar. A solution of conc. HCl and water (1:1) was added to the flask to give a cloudy orange solution. The reaction mixture was stirred under reflux for 4 h to produce a clear, deep orange solution. The reaction mixture was cooled down to room temperature, basified to pH 11 with a 10% solution of sodium hydroxide and extracted with ethyl acetate (3 × 20 mL). The combined organic layers were dried over MgSO₄, evaporated in vacuo, and then evacuated overnight under a high vacuum to give diketone-diamine 7 (88.7 mg, 50%) as a brown powder. mp 150 °C (under air, decomposed to black solid). $R_f = 0.46$ (diethyl ether, regular TLC plate). ¹H NMR (400 MHz, dimethyl sulfoxide-*d*₆): $\delta = 7.981$ (s, 1H), 7.028 (s, 2H), 5.803 (s, 1H), 2.388 (s, 4H), 1.192 (s, 12H); unidentified impurities: $\delta = 8.102, 7.544, 6.496, 4.015, \text{ and } 1.982$ ppm with a relative integration approximately 5 mol %. ¹³C NMR (100 MHz, dimethyl sulfoxide-*d*₆): $\delta = 191.34, 154.34, 127.79, 109.67, 94.90, 52.16, 49.94, 27.47$. IR (cm⁻¹): 3329, 3318, 2966, 2875, 1646, 1601, 1536, 1278. HR-ESI MS (0.05% NaOAc in MeOH/H₂O (3:1)): m/z ion type (%RA for $m/z = 284\text{--}306$): 295.1411 [M + Na]⁺ (100%, -3.9 ppm for ¹²C₁₆¹H₂₀¹⁴N₂¹⁶O₂²³Na₁).

Preparation of 8. Diketone-diamine 7 (450.0 mg, 1.64 mmol, 1 equiv) was evacuated in a Schlenk vessel under a high vacuum overnight. Allylmagnesium bromide (1.0 M in ether, 33 mL, 32.8 mmol, 20 equiv) was added to the Schlenk vessel to produce a purple colored solution. After 5 min of stirring, the color of the solution changed to orange. The reaction mixture was stirred at 40 °C for 72 h. The crude reaction mixture was diluted with diethyl ether (20 mL), and then methanol (1 mL) was added dropwise at 0 °C. The crude product was extracted with water (2 × 50 mL), NH₄Cl solution (1 × 50 mL), and brine (1 × 50 mL). The combined organic layers were dried over Na₂SO₄ and evaporated in vacuo. The crude product was evacuated on a high vacuum overnight and purified by column

chromatography (30% diethyl ether in pentane) to give diamine **8** (131.0 mg, 20%) as sticky dark yellow oil. $R_f = 0.30$ (30% diethyl ether/pentane, 3% deactivated TLC). $^1\text{H NMR}$ (600 MHz, acetone- d_6): $\delta = 6.948$ (s, 1H), 5.770–5.684 (m, 5H), 5.028–4.979 (m, 8H), 4.143 (br, 2H), 2.490–2.389 (m, 8H), 1.679 (s, 4H), 1.188 (s, 12H). $^{13}\text{C NMR}$ (150 MHz, acetone- d_6): $\delta = 144.38, 137.14, 126.32, 117.46, 117.43, 101.36, 49.83, 46.98, 43.90, 38.67, 31.43$. IR (cm^{-1}): 3363, 3072, 2972, 2956, 2922, 2859, 1636, 1620, 1511, 1438, 1381, 1363, 1315, 1285, 1234, 1189, 1176, 996, 910, 824. HR-ESI MS (0.1% HCOOH in MeOH): m/z ion type (%RA for $m/z = 400$ –410): 405.3262 $[\text{M} + \text{H}]^+$ (100%, -1.9 ppm for $^{12}\text{C}_{28}^{14}\text{H}_{41}^{14}\text{N}_2$).

Preparation of 9. A clear yellow solution of diamine **8** (26.0 mg, 0.0643 mmol, 1 equiv) in 2 mL of ethanol was transferred into a Schlenk vessel equipped with a magnetic stirring bar. Pd/C was added into the Schlenk vessel to produce a suspension. The Schlenk vessel was evacuated briefly using a diaphragm pump and charged with hydrogen gas. The reaction was stirred at room temperature until completion. The crude product was filtered through a Celite plug with ethyl acetate, evaporated under reduced pressure and subsequently evacuated on a high vacuum overnight to produce diamine **9** (25.3 mg, 95%) as a light yellow solid. The crude product was washed with a small portion (3–4 drops) of methanol (3 times) to yield diamine **9** as a white solid, used for characterization. mp 91–92 °C (under air). $R_f = 0.30$ (30% diethyl ether/pentane, 3% deactivated TLC). $^1\text{H NMR}$ (400 MHz, acetone- d_6): $\delta = 6.763$ (s, 1H), 5.696 (s, 1H), 4.007 (br, 2H), 1.655 (s, 4H), 1.610–1.556 (m, 8H), 1.263–1.202 (m, 8H), 1.176 (s, 12H), 0.847 (t, $J = 7.2$ Hz, 12H). $^{13}\text{C NMR}$ (100 MHz, acetone- d_6): $\delta = 144.04, 125.59, 118.84, 101.39, 49.91, 45.62, 44.44, 38.84, 31.52, 18.14, 15.29$. IR (ZnSe, cm^{-1}): 3350, 2955, 2931, 2870, 1622, 1510, 1456, 1380, 1362, 1315, 1230, 1190, 822. HR-ESI MS (MeOH:H₂O, 3:1): m/z ion type (%RA for $m/z = 410$ –420): 413.3888 $[\text{M} + \text{H}]^+$ (100%, -1.9 ppm for $^{12}\text{C}_{28}^{14}\text{H}_{49}^{14}\text{N}_2$).

Preparation of 10. NBS (14.3 mg, 0.0805 mmol) in degassed chloroform (1 mL) was added dropwise to a solution of diamine **9** (30.2 mg, 0.0732 mmol) with NaHCO₃ (74.3 mg, 0.878 mmol) and anhydrous Na₂SO₄ (124.7 mg, 0.878 mmol) in degassed chloroform (3 mL) at -40 °C under N₂ atmosphere to produce a heterogeneous orange solution. After stirring at -40 °C for 1 h, an excess of Na₂S₂O₅ was added and then the reaction mixture was allowed to attain room temperature and was stirred for additional 10 min. After the solids were filtered off, the filtrate was concentrated in vacuo to yield a brown oil. The crude product was filtered through a short plug of silica gel and eluted with 30% diethyl ether/pentane to give a brown film. A small portion of MeOH (3 drops) was added to the brown film and evaporated under N₂ to give bromodiamine **10** (30.5 mg, 85%) as a brown semisolid. $R_f = 0.67$ (4% diethyl ether/pentane, 3% deactivated TLC). $^1\text{H NMR}$ (600 MHz, acetone- d_6): $\delta = 6.868$ (s, 1H), 4.186 (br, 1H), 1.727 (s, 4H), 1.621 (m, 8H), 1.292–1.187 (m, 8H), 1.261 (s, 12H), 0.850 (t, $J = 7.2$ Hz, 12H); unidentified impurities: $\delta = 7.627, 6.950, 5.611, 4.698, \text{ and } 4.644$ ppm with a relative integration approximately 3 mol %. $^{13}\text{C NMR}$ (100 MHz, acetone- d_6): $\delta = 140.28, 124.71, 119.52, 98.38, 50.62, 45.24, 43.98, 39.55, 31.88, 18.13, 15.22$. IR (ZnSe, cm^{-1}): 3384, 2955, 2931, 2870, 1612, 1483, 1466, 1425, 1382, 1363, 1290, 1230, 1200, 1182, 1108, 743. HR-ESI MS (MeOH:H₂O, 3:1): m/z ion type (%RA for $m/z = 488$ –497): 490.2903 $[\text{M}]^+$ (100%, -4.0 ppm for $^{12}\text{C}_{28}^{14}\text{H}_{47}^{14}\text{N}_2^{79}\text{Br}_1$), 492.2922 $[\text{M}]^+$ (80%, 4.0 ppm for $^{12}\text{C}_{28}^{14}\text{H}_{47}^{14}\text{N}_2^{81}\text{Br}_1$).

Preparation of 11. Bromodiamine **10** (54.3 mg, 110 μmol) and 4-*tert*-butylphenylboronic acid (29.5 mg, 165 μmol , 1.5 equiv) were placed into a Schlenk vessel under N₂ atmosphere. Pd(PPh₃)₄ (25.4 mg, 22.0 μmol , 10 mol %) was added to the vessel in a glovebag under N₂ atmosphere. Benzene (2 mL), ethanol (0.6 mL), and aqueous Na₂CO₃ (1 M, 0.6 mL) were bubbled with N₂ for 10 min, and then added to the reaction vessel. The reaction mixture was stirred at 90 °C for 72 h, then poured into distilled water and subsequently extracted with benzene. The combined organic layers were washed with 2 M NaOH solution (5 \times 4 mL) and brine (3 \times 4 mL). The combined organic phase was dried over anhydrous Na₂SO₄, and then concentrated in vacuo to provide the crude product as a colorless film. The crude mixture was filtered through a short plug of Celite and silica

gel with 10% diethyl ether/pentane. The filtrate was evaporated under reduced pressure and evacuated under a high vacuum overnight. The crude product was then purified by PTLC (5% diethyl ether/pentane) to give 4-*tert*-butylphenyldiamine **11** as a white solid (35.6 mg, 59%). mp 120–121 °C (under air). $R_f = 0.36$ (3% diethyl ether/pentane, 3% deactivated TLC). $^1\text{H NMR}$ (400 MHz, acetone- d_6): $\delta = 7.570$ (d, $J = 8.4$ Hz, 2H), 7.125 (d, $J = 8.4$ Hz, 2H), 6.878 (s, 1H), 3.034 (br, 2H), 1.697–1.567 (m, 8H), 1.664 (s, 4H), 1.367 (s, 9H), 1.310–1.217 (m, 8H), 1.059 (s, 12H), 0.869 (t, $J = 7.2$ Hz, 12H). $^1\text{H NMR}$ (500 MHz, benzene- d_6): $\delta = 7.433$ (d, $J = 8.0$ Hz, 2H), 7.381 (d, $J = 8.5$ Hz, 2H), 7.161 (s, 1H), 3.322 (br, 2H, exch. D₂O), 1.865–1.739 (m, 8H), 1.689 (s, 4H), 1.445–1.363 (m, 8H), 1.154 (s, 9H), 1.015 (s, 12H), 0.944 (t, $J = 7.5$ Hz, 12H). ^1H – ^{15}N HSQC (acetone- d_6): δ (^{15}N) = -287.9 ppm. $^{13}\text{C NMR}$ (150 MHz, acetone- d_6 , LB = -0.2 Hz, GB = 0.5 Hz): $\delta = 151.04, 140.80, 140.77, 134.47, 132.02, 132.01, 127.48, 124.75, 119.28, 119.26, 113.67, 50.33, 50.24, 45.40, 45.38, 44.69, 44.66, 39.29, 35.24, 31.79, 31.75, 18.22, 15.29$. IR (cm^{-1}): 3379, 3084, 3027, 2953, 2930, 2869, 1605, 1476, 1456, 1380, 1361, 1268, 1228, 1201, 1179. HR-ESI MS (MeOH:H₂O, 3:1): m/z ion type (%RA for $m/z = 543$ –548): 544.4769 $[\text{M}]^+$ (100%, 2.3 ppm for $^{12}\text{C}_{38}^{16}\text{H}_{60}^{14}\text{N}_2$).

General Procedure for the Generation of 2. Diamine **11** (0.70–1.32 mg, 1.28–2.42 μmol) was placed in a custom-made Schlenk-EPR-tube (5 mm OD) and then it was placed under a high vacuum (10^{-4} mTorr). The whole EPR sample tube was wrapped with heating tape and heated at 70 °C overnight. The next day, the heating tape was removed in the sample area and the remaining part of EPR tube was heated at 110 °C overnight. THF (~ 0.1 mL, ~ 10 mm height) was added to the vessel by vacuum transfer, and then the solution was stirred for 30 min at -30 °C. *n*-BuLi (0.14–0.26 M in hexane, 12–27 μL , 3.08–5.81 μmol , 2.4 equiv) was added to produce the corresponding dianion. After stirring at -30 °C for 3–5 h, the orange reaction mixture was evaporated at -45 °C and then immersed in liquid nitrogen. 2-MeTHF (~ 0.1 mL) was added to the reaction mixture by vacuum transfer, and then the reaction mixture (under a vacuum) was immersed in liquid nitrogen. Subsequently, iodine was vacuum transferred to the sample tube wall, just above the reaction mixture. Iodine was mixed into the reaction mixture at -115 °C, and then the green solution was stirred at -115 °C for 1 h. The resultant green solution was stored in liquid nitrogen; EPR spectra were obtained at 132 K.

General Procedure for the Measurements of χT for Statistical Analyses for 1 and 2. After obtaining the samples using the protocol described in the generation of 2, 2-MeTHF was added by vacuum transfer at liquid N₂ temperature, to obtain ~ 4 –5 cm height solution in the EPR tube. The resultant solution was mixed by hand with a stirbar (and external magnet) for additional 15–30 min at -115 °C, and then EPR spectra at 132 K were taken. Two EPR spectra for both the sample and the nitroxide reference were obtained and their double integrations were averaged, separately for the sample and for the reference. Subsequently, the sample and the reference were annealed at -115 and 22 °C, respectively. Following the annealing, the sample and the reference were frozen carefully with liquid N₂ to give a continuous (and bubble-free) block of 2-MeTHF glass, prior to placing the sample and the reference in the EPR cavity for another set of spectra. Overall, $n = 5$ –6 of independent sets of spectra were obtained for each of the three samples of 2 and their references (Table 3). The EPR spectra for 1 were obtained using the samples contained in the SQUID tubes; $n = 4$ sets of spectra were obtained for each of the two samples (Table 4).

General Procedure for Decay Kinetics Measurements for 1 and 2. After obtaining the samples using the protocol described in the generation of 2, 2-MeTHF was added by vacuum transfer to obtain a ~ 3.5 –5 cm height solution in EPR tube. EPR spectra of the diluted samples were taken at 132 K. Then, the samples were annealed at -78 °C, -27 °C, and 22 °C. For reference, EPR spectra of TEMPONE or TEMPOL (1 mM in 2-MeTHF) were taken at 132 K. A similar protocol was implemented for the sample of 1.

■ ASSOCIATED CONTENT

■ Supporting Information

General procedures and materials, additional experimental details, X-ray crystallographic files for **7** and **11** in CIF format, and complete ref 24. This material is available free of charge via the Internet at <http://pubs.acs.org>.

■ AUTHOR INFORMATION

Corresponding Author

arajca1@unl.edu

Notes

The authors declare no competing financial interest.

■ ACKNOWLEDGMENTS

We thank the National Science Foundation for support of this research through Grants CHE-1012578 and CHE-1362454, including the purchase of the Electron Paramagnetic Resonance (EPR) spectrometer (DMR-0216788) used in this work. ChemMatCARS Sector 15 is principally supported by the Divisions of Chemistry (CHE) and Materials Research (DMR), National Science Foundation, under Grant Number NSF/CHE-1346572. Use of the Advanced Photon Source was supported by the U.S. Department of Energy, Office of Science, Office of Basic Energy Sciences, under Contract No. DE-AC02-06CH11357. We thank Benjamin Enns for his help with the synthesis of diamine **7**, and for his support through the National Science Foundation REU site (CHE-1156560).

■ REFERENCES

- (1) Rajca, A.; Olankitwanit, A.; Rajca, S. *J. Am. Chem. Soc.* **2011**, *133*, 4750–4753.
- (2) Wenthold, P. G.; Kim, J. B.; Lineberger, W. C. *J. Am. Chem. Soc.* **1997**, *119*, 1354–1359.
- (3) Haider, K. W.; Migirdicyan, E.; Platz, M. S.; Soundararajan, N.; Despres, A. *J. Am. Chem. Soc.* **1990**, *112*, 733–738.
- (4) Abe, M. *Chem. Rev.* **2013**, *113*, 7011–7088.
- (5) Lineberger, W. C.; Borden, W. T. *Phys. Chem. Chem. Phys.* **2011**, *13*, 11792–11813.
- (6) (a) Ratera, I.; Veciana, J. *Chem. Soc. Rev.* **2012**, *41*, 303–349. (b) Lahti, P. M. *Adv. Phys. Org. Chem.* **2011**, *45*, 93–169. (c) Shishlov, N. M. *Russ. Chem. Rev.* **2006**, *75*, 863–884. (d) Rajca, A. *Adv. Phys. Org. Chem.* **2005**, *40*, 153–199. (e) Rajca, A. *Chem.—Eur. J.* **2002**, *8*, 4834–4841. (f) Rajca, A. *Chem. Rev.* **1994**, *94*, 871–893.
- (7) (a) Rajca, S.; Rajca, A.; Wongsriratanakul, J.; Butler, P.; Choi, S. *J. Am. Chem. Soc.* **2004**, *126*, 6972–6986. (b) Rajca, A.; Wongsriratanakul, J.; Rajca, S. *J. Am. Chem. Soc.* **2004**, *126*, 6608–6626. (c) Rajca, A.; Wongsriratanakul, J.; Rajca, S.; Cerny, R. L. *Chem.—Eur. J.* **2004**, *10*, 3144–3157. (d) Rajca, A.; Lu, K.; Rajca, S. *J. Am. Chem. Soc.* **1997**, *119*, 10335–10345. (e) Rajca, A.; Rajca, S.; Padmakumar, R. *Angew. Chem., Int. Ed. Engl.* **1994**, *33*, 2091–2093.
- (8) (a) Rajca, A.; Wongsriratanakul, J.; Rajca, S. *Science* **2001**, *294*, 1503–1505. (b) Rajca, A.; Rajca, S.; Wongsriratanakul, J. *J. Am. Chem. Soc.* **1999**, *121*, 6308–6309.
- (9) Boratynski, P. J.; Pink, M.; Rajca, S.; Rajca, A. *Angew. Chem., Int. Ed.* **2010**, *49*, 5459–5462.
- (10) (a) Rajca, A.; Shiraishi, K.; Vale, M.; Han, H.; Rajca, S. *J. Am. Chem. Soc.* **2005**, *127*, 9014–9020. (b) Rajca, A.; Utamapanya, S. *J. Org. Chem.* **1992**, *57*, 1760–1767.
- (11) (a) Rajca, A.; Olankitwanit, A.; Wang, Y.; Boratynski, P. J.; Pink, M.; Rajca, S. *J. Am. Chem. Soc.* **2013**, *135*, 18205–18215. (b) Swager, T. M.; Azzarelli, J. M. *Synfacts* **2014**, *10*, 0142.
- (12) (a) Suzuki, S.; Furui, T.; Kuratsu, M.; Kozaki, M.; Shiomi, D.; Sato, K.; Takui, T.; Okada, K. *J. Am. Chem. Soc.* **2010**, *132*, 15908–15910. (b) Fukuzaki, E.; Nishide, H. *J. Am. Chem. Soc.* **2006**, *128*, 996–1001.
- (13) Davis, R. M.; Sowers, A. L.; DeGraff, W.; Bernardo, M.; Theftford, A.; Krishna, M. C.; Mitchell, J. B. *Free Radical Biol. Med.* **2011**, *51*, 780–790.
- (14) (a) Rajca, A.; Wang, Y.; Boska, M.; Paletta, J. T.; Olankitwanit, A.; Swanson, M. A.; Mitchell, D. G.; Eaton, S. S.; Eaton, G. R.; Rajca, S. *J. Am. Chem. Soc.* **2012**, *134*, 15724–15727. (b) Correction for ref 14a: Rajca, A.; Wang, Y.; Boska, M.; Paletta, J. T.; Olankitwanit, A.; Swanson, M. A.; Mitchell, D. G.; Eaton, S. S.; Eaton, G. R.; Rajca, S. *J. Am. Chem. Soc.* **2014**, *136*, 3318–3318. (c) Spagnol, G.; Shiraishi, K.; Rajca, S.; Rajca, A. *Chem. Commun.* **2005**, 5047–5049.
- (15) Clore, G. M.; Iwahara, J. *Chem. Rev.* **2009**, *109*, 4108–4139.
- (16) (a) Herrmann, C.; Solomon, G. C.; Ratner, M. A. *J. Am. Chem. Soc.* **2010**, *132*, 3682–3684. (b) Jahn, B. O.; Ottosson, H.; Galperin, M.; Fransson, J. *ACS Nano* **2013**, *7*, 1064–1071.
- (17) Amiri, S.; Schreiner, P. R. *J. Phys. Chem. A* **2009**, *113*, 11750–11757.
- (18) (a) The results referred to as broken symmetry DFT (BS-DFT) in Figure 1 are summarized in Table S14, Supporting Information. (b) For *m*-xylylene, the EOM-SF-CCSD computations, see: Wang, T.; Krylov, A. I. *J. Chem. Phys.* **2005**, *123*, 104304–1–6. (c) For *m*-xylylene, the CASPN2T computations, see: Hrovat, D. A.; Murcko, M. A.; Lahti, P. M.; Borden, W. T. *J. Chem. Soc., Perkin Trans. 2* **1998**, *5*, 1037. (d) For DDCI computations for **1a**, see: Barone, V.; Boilleau, C.; Cacelli, L.; Ferretti, A.; Monti, S.; Prampolini, G. *J. Chem. Theory Comput.* **2013**, *9*, 300–307.
- (19) Pisaneschi, F.; Sejberg, J. J. P.; Blain, C.; Ng, W.-H.; Aboagye, E. O.; Spivey, A. C. *Synlett* **2011**, 241–244.
- (20) Donnelly, J. A.; Farrell, D. F. *J. Org. Chem.* **1990**, *55*, 1757–1761.
- (21) Rajca, A.; Shiraishi, K.; Pink, M.; Rajca, S. *J. Am. Chem. Soc.* **2007**, *129*, 7232–7233.
- (22) (a) Eliel, E. L.; Wilen, S. H. *Stereochemistry of Organic Compounds*; Wiley: New York, 1994; pp 726–730. (b) Auf der Heyde, W.; Luttko, W. *Chem. Ber.* **1978**, *111*, 2384–2395.
- (23) (a) Rajca, A.; Boratynski, P. J.; Olankitwanit, A.; Shiraishi, K.; Pink, M.; Rajca, S. *J. Org. Chem.* **2012**, *77*, 2107–2120. (b) Rajca, A.; Shiraishi, K.; Boratynski, P. J.; Pink, M.; Miyasaka, M.; Rajca, S. *J. Org. Chem.* **2011**, *76*, 8447–8457.
- (24) Frisch, M. J. et al. *Gaussian 09*, Revision A.01; Gaussian, Inc.: Wallingford, CT, 2009.
- (25) Structures of **11a** and **12a** were optimized with their lateral six- and five-membered rings of the fused tricyclic moieties in the *anti*-conformations, e.g., for **11a**, *anti*-half-chairs (Table S13, Supporting Information).
- (26) Jain, R.; Bally, T.; Rablen, P. R. *J. Org. Chem.* **2009**, *74*, 4017–4023.
- (27) Saielli, G.; Nicolaou, K. C.; Ortiz, A.; Zhang, H.; Bagno, A. *J. Am. Chem. Soc.* **2011**, *133*, 6072–6077.
- (28) Barone, G.; Gomez-Paloma, L.; Duca, D.; Silvestri, A.; Riccio, R.; Bifulco, G. *Chem.—Eur. J.* **2002**, *8*, 3233–3239.
- (29) (a) Willoughby, P. H.; Jansma, M. J.; Hoyer, T. R. *Nat. Protoc.* **2014**, *9*, 643–660. (b) Lodewyk, M. W.; Siebert, M. R.; Tantillo, D. J. *Chem. Rev.* **2012**, *112*, 1839–1862.
- (30) Rosokha, S. V.; Kochi, J. K. *Acc. Chem. Res.* **2008**, *41*, 641–653.
- (31) Neugebauer, F. A.; Fischer, H.; Bamberger, S.; Smith, H. O. *Chem. Ber.* **1972**, *105*, 2694–2713.
- (32) Morita, Y.; Suzuki, S.; Fukui, K.; Nakazawa, S.; Kitagawa, H.; Kishida, H.; Okamoto, H.; Naito, A.; Sekine, A.; Ohashi, Y.; Shiro, M.; Sasaki, K.; Shiomi, D.; Sato, K.; Takui, T.; Nakasuji, K. *Nat. Mater.* **2008**, *7*, 48–51.
- (33) Rajca, A.; Rajca, S.; Desai, S. R. *J. Am. Chem. Soc.* **1995**, *117*, 806–816.
- (34) The apparent broadening of the outermost pentuplets is greater in **2**, compared to that in **1**, presumably, due to smaller $|A_{ZZ}/2hcl$ in **2** and distribution of conformations associated with the “half-chairs” in **2**.
- (35) Morton, J. R. *Chem. Rev.* **1964**, *64*, 453–471.
- (36) The spin-orbit coupling contribution to the *D*-tensor may be neglected in the *N*-centered π -diradicals: Havlas, Z.; Křivá, M.; Michl. *J. Mol. Phys.* **2005**, *103*, 407–411.

- (37) (a) Rajca, A.; Shiraishi, K.; Rajca, S. *Chem. Commun.* **2009**, 4372–4374. (b) Rajca, A.; Takahashi, M.; Pink, M.; Spagnol, G.; Rajca, S. *J. Am. Chem. Soc.* **2007**, *129*, 10159–10170.
- (38) (a) Roberts, J. R.; Ingold, K. U. *J. Am. Chem. Soc.* **1973**, *95*, 3228–3235. (b) Blanksby, S. J.; Ellison, G. B. *Acc. Chem. Res.* **2003**, *36*, 255–263.
- (39) (a) Soda, T.; Kitagawa, Y.; Onishi, T.; Takano, Y.; Shigeta, Y.; Nagao, H.; Yoshioka, Y.; Yamaguchi, K. *Chem. Phys. Lett.* **2000**, *319*, 223. (b) Yamaguchi, K.; Jensen, F.; Dorigo, A.; Houk, K. N. *Chem. Phys. Lett.* **1988**, *149*, 537–542.
- (40) Noodleman, L.; Case, D. A. *Adv. Inorg. Chem.* **1992**, *38*, 423–470.
- (41) Trinquier, G.; Suaud, N.; Malrieu, J.-P. *Chem.—Eur. J.* **2010**, *16*, 8762–8772.
- (42) Mañeru, D. R.; Pal, A. K.; Moreira, I. P. R.; Datta, S. N.; Illas, F. *J. Chem. Theory Comput.* **2014**, *10*, 335–345.
- (43) Neese, F. *ORCA—An Ab Initio, Density Functional and Semiempirical Program Package*, Version 2.6; University of Bonn: Bonn, Germany, 2008.
- (44) Sinnecker, S.; Neese, F. *J. Phys. Chem. A* **2006**, *110*, 12267–12275.
- (45) *SAINT*; Bruker Analytical X-Ray Systems: Madison, WI, 2011.
- (46) Blessing, R. *Acta Crystallogr., Sect. A: Found. Crystallogr.* **1995**, *51*, 33–38.
- (47) Burla, M. C.; Caliandro, R.; Carnalli, M.; Carrozzini, B.; Cascarano, G. L.; De Caro, L.; Giacovazzo, C.; Polidori, G.; Sagna, R. *Sir2004, A Program for Automatic Solution and Refinement of Crystal Structure*, Version 1.0; Institute of Crystallography: Bari, Italy, 2004.
- (48) (a) *SHELXTL-Plus*, Version 5.10; Bruker Analytical X-Ray Systems: Madison, WI, 2008. (b) Sheldrick, G. M. *Acta Crystallogr., Sect. A: Found. Crystallogr.* **2008**, *64*, 112–122.
- (49) Spagnol, G.; Rajca, A.; Rajca, S. *J. Org. Chem.* **2007**, *72*, 1867–1869.